energies

MDPI

Article

Investigations of Rake and Rib Structures in Sand Traps to Prevent Sediment Transport in Hydropower Plants

Mads Mehus Ivarson [1], Chirag Trivedi [1,*] and Kaspar Vereide [2,3]

[1] Waterpower Laboratory, NTNU—Norwegian University of Science and Technology, Alfred Getz' vei 4, 7034 Trondheim, Norway; mads.ivarson@ntnu.no
[2] Department of Civil and Environmental Engineering, NTNU—Norwegian University of Science and Technology, 7031 Trondheim, Norway; kaspar.vereide@ntnu.no
[3] Sira-Kvina kraftselskap, Stronda 12, 4440 Tonstad, Norway
* Correspondence: chirag.trivedi@ntnu.no

Abstract: In order to increase the lifespan of hydraulic turbines in hydropower plants, it is necessary to minimize damages caused by sediment erosion. One solution is to reduce the amount of sediments by improving the design of sand trap. In the present work, the effects on sand trap efficiency by installing v-shaped rake structures for flow distribution and rib structures for sediment trapping is investigated numerically using the SAS–SST turbulence model. The v-shaped rake structures are located in the diffuser near the inlet of the sand trap, while the ribs cover a section of the bed in the downstream end. Three-dimensional models of the sand trap in Tonstad hydropower plant are created. The present study showed that integrating rib type structure can reduce the total weight of sediments escaping the sand trap by 24.5%, which leads to an improved sand trap efficiency. Consequently, the head loss in the sand trap is increased by 1.8%. By additionally including the v-shaped rakes, the total weight of sediments escaping the sand trap is instead increased by 48.5%, thus worsening the sand trap efficiency. This increases head loss by 12.7%. The results also show that turbulent flow commencing at the sand trap diffuser prevents the downstream settling of sediments with a diameter of less than one millimeter. The hydraulic representation of the numerical model is validated by comparison with particle image velocimetry measurements of the flow field from scale experiments and ADCP measurements from the prototype. The tested rib design has not previously been installed in a hydropower plant, and can be recommended. The tested v-shaped rakes have been installed in existing hydropower plants, but this practice should be reconsidered.

Keywords: hydropower; CFD; sand trap; sediment transport; particle; multiphase

check for updates

Citation: Ivarson, M.M.; Trivedi, C.; Vereide, K. Investigations of Rake and Rib Structures in Sand Traps to Prevent Sediment Transport in Hydropower Plants. *Energies* **2021**, *14*, 3882. https://doi.org/10.3390/en14133882

Academic Editors: John M. Cimbala and Bryan J. Lewis

Received: 1 June 2021
Accepted: 23 June 2021
Published: 28 June 2021

Publisher's Note: MDPI stays neutral with regard to jurisdictional claims in published maps and institutional affiliations.

Copyright: © 2021 by the authors. Licensee MDPI, Basel, Switzerland. This article is an open access article distributed under the terms and conditions of the Creative Commons Attribution (CC BY) license (https://creativecommons.org/licenses/by/4.0/).

1. Introduction

Sediment handling and erosion in hydropower plants have been long-standing engineering challenges. Hydropower plants are often upgraded and refurbished to improve performance and plant capacity. Sediment handling in hydropower plants can be done through catchment manipulation, dam and intake design, tunnel lining, sand traps, and turbine design. The motivation of the work is the upgrading and refurbishment of existing hydropower plants. After upgrading their installed capacity, several large Norwegian hydropower plants experienced operational problems associated with sediments entering the penstock and causing erosion to the turbine [1]. Moreover, a higher variability in power demand in recent years has led to some plants converting from base-load to peak-load production. This results in variable discharge through the tunnels, which stirs up sediments from the tunnel bed in unlined tunnels with remaining rock material on the invert, which is typical in Norwegian hydropower plants. Currently, the power plant does not have a system to indicate how much sediment actually passes through the sand trap and is transported through the turbine. To the authors experience, this is the typical situation for hydropower sand traps. For comparison, the records of removed sediments since 2015 are

in the range from 150 m^3 to 15 m^3 per year, with a decreasing trend. Sediments can cause damage to the turbine through abrasion on the turbine surfaces. Larger particles may also cause larger dents on the turbines. Such damage results in reduced turbine efficiency and reduced structural integrity of the turbine components. The damage may, in turn, trigger increased cavitation that accelerates the degradation [2,3].

Tonstad hydropower plant, located in the mountains of southwestern Norway, is currently experiencing such challenges. In 1988, the plant upgraded its capacity from 640 to 960 MW by installing a new 320 MW Francis turbine. An additional penstock, surge tank, and sand trap were built. However, the unlined headrace tunnel was left untouched. It was expected that the higher discharge required to run all three turbines would lead to an increased amount of sand and rocks to be flushed into the turbines. However, the actual amount of sediments being transported with the flow was surprisingly large. One of the reasons for the increased amount of sediment transport is the poor design of the sand trap, which was designed in the 1960s and is now underperforming.

Figure 1 shows the layout of a typical high-head hydropower plant. A sand trap is a section of the water way, typically located immediately upstream of the penstock. This allows the headrace tunnel, with the remaining stone and sand material after its construction, to be unlined. Sand traps are designed to reduce flow velocity, which allows sediments to settle easier. The velocity is typically reduced by 30 to 50% [1]. This is done by increasing the cross-sectional area of the tunnel. The main challenge is poor performance of sand trap, which is intended to trap sediments before they reach the penstock. A proposal to improve sand trap performance is to cover sections of the bed with concrete ribs. This has been shown in physical experiments to create a low-velocity zone beneath the ribs, protecting sediments on the bed from being stirred up, while also allowing sediments to fall through the gaps between ribs [4,5]. Another proposal is to install rows of v-shaped rakes in the diffuser at the sand trap inlet. Increased levels of turbulence, such as those induced by these v-shaped rakes, has been shown to increase sediment settling speeds for certain particle sizes in numerical studies by Maxey in 1987 [6] and Wang and Maxey in 1993 [7]. This was later confirmed in physical experiments by Aliseda et al. in 2002 [8]. In these studies, sediments were found to settle in the peripheries of local vortex structures, which is coupled to a sweeping of sediments in directions normal to the flow.

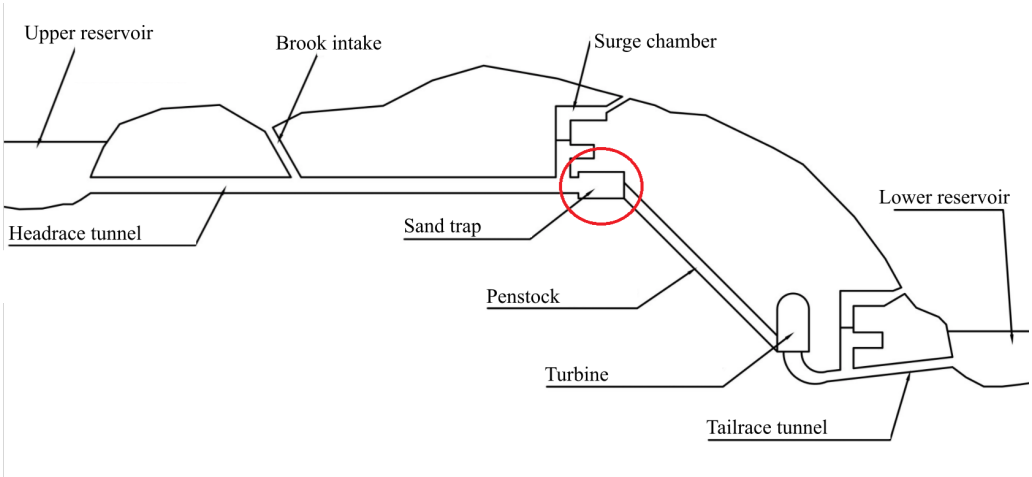

Figure 1. Layout of a typical high-head hydropower plant. The sand trap is marked with red color.

Several scientific studies have been conducted on the topic of sediment transport in hydropower sand traps. Olsen and Skoglund modelled the flow of water and sediment in a three-dimensional sand trap geometry using the $k - \epsilon$ turbulence model [9]. After including modifications to the turbulence model, both the flow field solution and sediment concentration calculations were in agreement with experimental procedures. Kjellesvig and Olsen modelled the bed changes in a sand trap using the transient convection–diffusion

equation for sediment concentration and an adaptive grid adjusting for changes in the bed [10]. Large amounts of sediments could be seen being moved through the geometry in the simulations. The results compared well to physical model tests. Bråtveit and Olsen used 3D computational fluid dynamics (CFD) simulations to calibrate horizontal acoustic Doppler current profilers (H-ADCP) in the Tonstad sand trap [11]. The study found that the 3D CFD simulations could accurately calibrate the H-ADCP while also assessing the flow conditions at the locations of installation. Almeland et al. computed water flow in a model of the Tonstad sand trap using different versions of the $k - \epsilon$ turbulence model [12]. Depending on the discretisation scheme, grid resolution, and turbulence model, the computations showed the flow field to follow both the left side, right side, and centre of the diffuser. Field measurements showed that the main current followed the centre of the diffuser.

The present work is part of an ongoing sand trap research project. In previous work by Richter et al., it was found that implementing ribs just upstream of the penstock increased sand trap efficiency dramatically, as sediments were trapped in the low-velocity zone underneath the ribs [4,5]. Havrevoll et al. performed PIV analyses on the flow around ribs in the sand trap to investigate sediment settling characteristics. They showed that ribs successfully separate the flow field [13]. Daxnerova performed experiments on a physical scale model of the sand trap at NTNU to determine the effects of installing various calming flow structure designs in the diffuser [14]. The best performing design from Daxnerova's research, a v-shaped rake type structure, will be further studied in this work.

The objective of the present work is to assess the changes in sand trap efficiency when including ribs in the downstream end of the sand trap. The effects on the turbulence dissipation and sediment trajectories by including v-shaped rakes in the diffuser will be investigated. The work aims to reproduce results from experiments on physical scale models of the sand trap in order to gain further confidence in the experimental results.

2. Materials and Methods

2.1. Sediment Transport Theory

When sediments at the tunnel bed are subjected to shear stresses higher than what is required to loosen them from the bed load, the sediments will be suspended and transported with the flow. Sediment transport can be divided into two main categories, depending on the shear velocity to settling velocity ratio of the particles, $u^* > w$ [15]. These categories are suspended load and bed load. Suspended load consists of finer particles that have low inertia and settling velocities due to their low mass. They are therefore transported further by the flow before settling compared with bed load sediments. Bed load usually consists of rocks and larger grains of sand that are too heavy to be suspended in water for longer durations. They are instead transported by sliding, saltating, or rolling along the sediment bed, as illustrated in Figure 2.

In order to determine if the upgrades improve sediment settling, it is necessary to measure the sand trap efficiency. The most straightforward method to compute the efficiency is a sediment-mass-based approach. Here, the ratio of the total mass of sediments injected at the inlet and escaped through the outlet is found. The efficiency can then be calculated as in Equation (1)

$$\eta = 1 - \frac{\Phi_{s,out}}{\Phi_{s,in}}, \tag{1}$$

where η is the sand trap efficiency and Φ represents the mass of sediment. Time-integrated particle mass flow reports created at the end of simulations will be used to find the inflow and outflow of sediments and then calculate sand trap efficiencies.

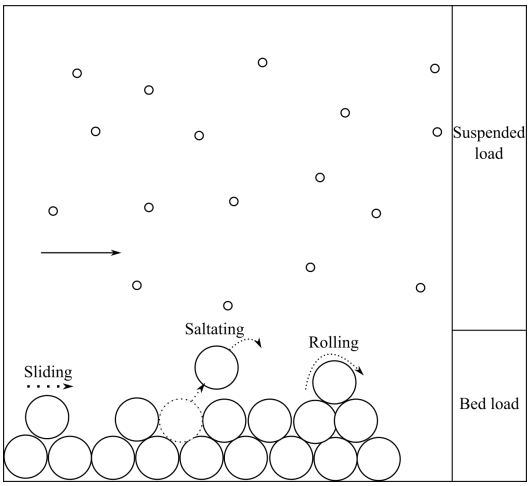

Figure 2. Types of sediment transport.

2.2. Head Loss

Installing new structures in the waterways could increase energy losses in the flow. This is mainly due to increased friction. This will affect the total head loss and, ultimately, the performance of the power plant. The head loss should therefore be minimised. Losses due to friction are determined by using the Darcy–Weisbach friction factor, seen in Equation (2).

$$h_f = f\frac{L \times v^2}{D \times 2g}, \tag{2}$$

where h_f (m) is the head loss, f is the dimensionless Darcy friction factor, L (m) is the length of the pipe, v (m/s) is the mean velocity of the flow, D (m) is the diameter of the tunnel, and g (m/s^2) is the gravitational acceleration. To ensure correct head loss calculations, it is important to find the correct Darcy friction factor. Using a Moody diagram, the friction factor can be found by determining the Reynolds number and relative roughness of the flow situation. In the present work, the Darcy–Weisbach equation form based on the pressure drop (Equation (3)) will be used to find the head loss caused by the upgrades.

$$\Delta h_L = \frac{\Delta p}{\rho g}, \tag{3}$$

where Δh_L is the head loss, Δp (Pa) is the pressure difference between two points, and ρ (kg/m^3) is the fluid density. The head loss in each of the geometries will be measured in post-processing. The head loss in the base case will be subtracted from each of the other cases, where the difference is the increased head loss caused by the upgrades.

2.3. Turbulence Modelling

To model the turbulent flow behaviour in the present work, the scale-adaptive simulation shear stress transport (SAS–SST) turbulence model was used. The model was found to perform better than the conventional RANS formulations in similar cases during the underlying project work. It introduces the Von Karman length scale into the turbulence scale equation to adapt to different turbulence structure sizes, while using base RANS equations in areas where the flow behaves more similar to steady state [16]. The SAS–SST are as follows:

$$\frac{\partial k}{\partial t} + \frac{\partial u_j k}{\partial x_j} = P_k - \beta^* \omega k + \frac{\partial}{\partial x_j}\left[(\nu + \frac{\nu_t}{\sigma_k})\frac{\partial k}{\partial x_j}\right] \tag{4}$$

$$\frac{\partial \omega}{\partial t} + \frac{\partial}{\partial x_j}(\overline{u}_j \omega) = \frac{\partial}{\partial x_j}\left[(\nu + \frac{\nu_t}{\sigma_\omega})\frac{\partial \omega}{\partial x_j}\right] - \beta\omega^2 + C_\omega + \alpha S^2(1 + P_{SAS}) \quad (5)$$

$$\nu_t \propto \frac{k}{\omega}, \quad P_{SAS} = \overline{\zeta}_2 \kappa \frac{L}{L_{vK,3D}}, \quad L_{vK,3D} = \kappa \frac{S}{U''}. \quad (6)$$

In these equations, S and U'' are generic first- and second-velocity derivatives, respectively. The SAS–SST model builds on the SST k-omega model by implementing an extra production term in the ω-equation, P_{SAS}. This term is attuned to transient fluctuations in the flow. In regions with a fine mesh where the flow is becoming unsteady, $L_{vK,3D}$ is reduced, increasing the production term. This will result in a large ω and, therefore, reduced k and ν_t values. In this way, the unsteadiness is not dampened, but is instead included as a part of the turbulence that is being resolved, leading to greater accuracy. A reduction of the turbulent viscosity dissipation occurs, which makes the momentum equations interpret the flow as transient rather than steady [17].

2.4. Computational Setup

The Tonstad power plant sand trap is 184 m-long, and the main tunnel has a cross-sectional area of around 9.9 m × 11 m (around 119 m^2). A picture of the prototype sand trap is shown in Figure 3. A 3D model of the sand trap is developed using engineering CAD software, see Figure 4. It was created from engineering drawings provided by the Sira-Kvina power company—the owner of the plant—and consists of a rectangular inlet section, a diffuser, a long tunnel section with a gentle slope, and a weir in the invert where the tunnel transitions into the penstock. This model is used as a base to add upgrades to in two other models. The additional models were created to test the effects of the upgrades, where one model includes only ribs and another includes both ribs and v-shaped rakes.

Figure 3. Picture of a prototype sand trap tunnel at hydropower plant; courtesy of Sira-Kvina kraftselskap.

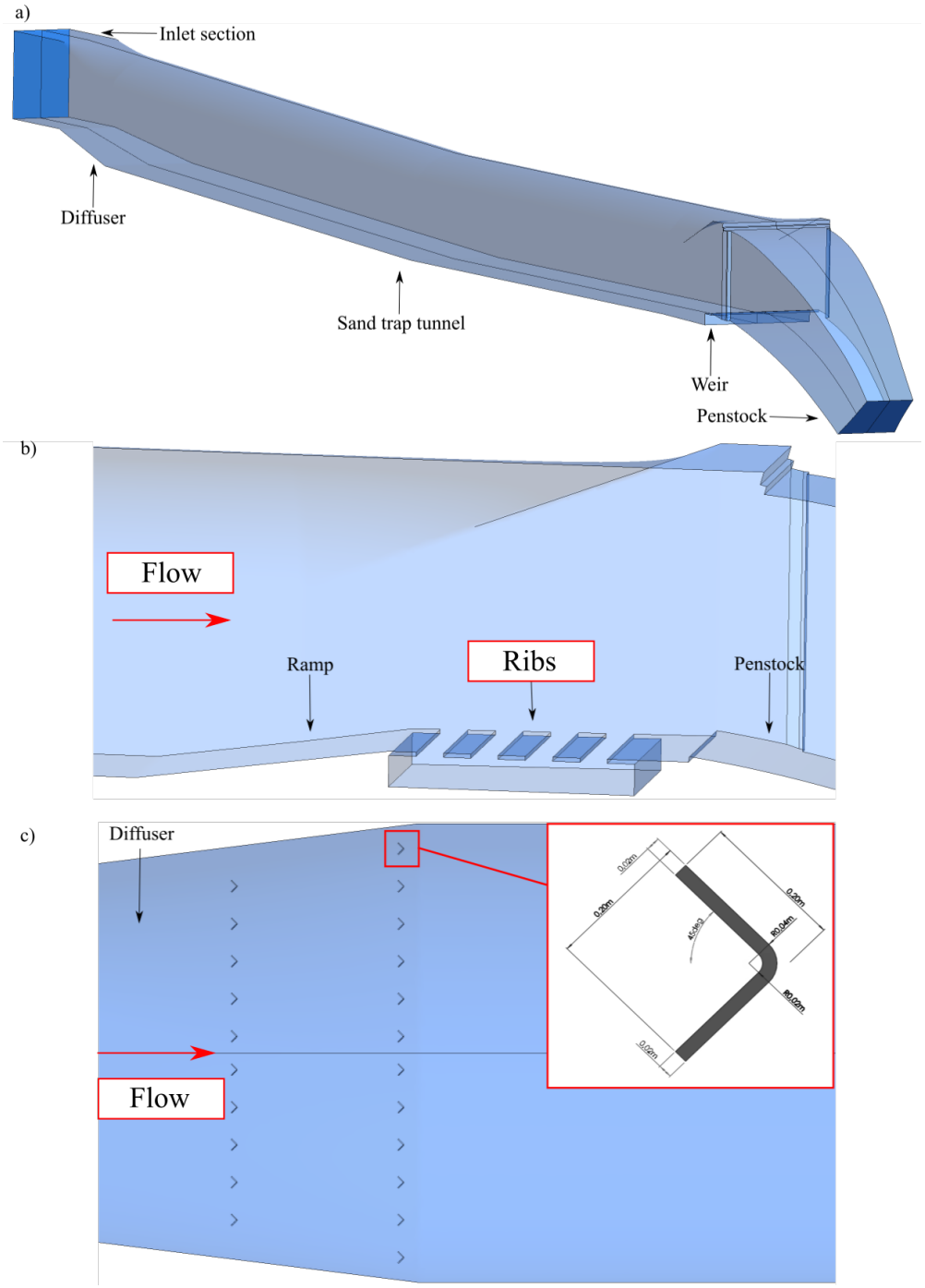

Figure 4. (**a**) Sand trap without upgrades. The distance from the end of the diffuser to the weir is 184 m. The diffuser is 16 m-long. The sand trap tunnel has a cross-sectional area of 119 m^2. (**b**) Ribs. The ribs are placed just upstream of the penstock, and are 1 m-wide and spaced 1 m-apart. The ramp has an 8% inclination. (**c**) Top view of the v-shaped rakes in the diffuser. The v-shaped rakes measure 6 m in height. Distances tip-to-tip between rakes are 1 m and 0.8 m for the upstream and downstream row, respectively. Zoomed part shows rake dimensions.

The ribs are placed just upstream of the penstock, in combination with the weir. This setup was tested in experiments [4,5]. The purpose of the ribs is to allow bed load sediments to fall between the ribs, while water is minimally affected. There are five ribs in total. The length of the ribs and the gap between ribs both measure 1 m. A ramp is placed upstream of the ribs to raise them above the bed and create space for sediments to accumulate. Further, in this way, excavating into the tunnel floor is not necessary. In

the work by Richter et al., the ramp was also found to protect sediments that had fallen between the ribs from being resuspended and flushed into the penstock.

The rake structure is made up of two rows of v-shaped rakes, with the tip of the rakes facing downstream. The rakes measure 6 m in height. Distances between rakes are 1 m and 0.8 m for the upstream and downstream row, respectively. The purpose of the rakes is to even the flow of the jet from the inlet and enhance the diffuser effect of slowing down the flow. The distance from the inlet to the rakes is 25 m, which is approximately 3 times the diameter. To ensure that stable and developed flow reaches the rakes, a distance of 5–10 times the inlet diameter is necessary. The fact that the flow reaching the rakes may not be fully developed in the simulations should be taken into consideration when analysing the results.

The three models of the sand trap are meshed similarly. In all three models, the diffuser and the invert are both given tetrahedral mesh structures, while the simpler geometries of the inlet section, tunnel, and penstock have structured hexahedral meshes. The number of cells in each mesh is >23 $\times$ 10^6. Inflation layers are added along the tunnel walls so that global $y^+ < 30$. This ensures accurate representation of flow conditions in the boundary layers. The mesh surrounding the ribs and the rakes are refined further to a maximum cell size of 0.01 m. Average element sizes in the diffuser, tunnel, and rib section are 1.05 mm, 1.39 mm, and 0.43 mm, respectively.

The chosen advection scheme is the "High Resolution" scheme available in CFX. This scheme is second-order accurate in smooth regions and reduces its order of accuracy in regions of high gradients, where unboundedness is a factor. A first-order-accurate scheme is generally more robust and reaches convergence criteria faster than a second-order-accurate scheme. However, this comes at the cost of higher numerical diffusion, resulting in a less-accurate solution. The transient scheme used is the Second-Order Backward Euler scheme.

Steady state multiphase simulations are run to create initial conditions for the transient multiphase simulations. The total simulated time for the transient simulations is set to allow sediments enough time to either reach the bed or exit through the outlet. The simulations use a discharge of 80 m^3/s, which is the discharge when the power plant is operating at design conditions. The inlet velocity boundary condition represents this mass flow rate. The wall roughness is 10^{-3} m in the numerical model. An overview of solution parameters and boundary conditions is presented in Table 1.

Table 1. Selected parameters and boundary conditions for unsteady simulations.

Parameters	Description
Mesh type	Structured hexahedral and unstructured tetrahedral.
Model scale	1:1 to prototype.
Analysis type	Transient: total time of 1000 s, time step of 0.5 s.
Fluid	Incompressible Newtonian fluid, water density and viscosity at 10 C
Boundary conditions	Inlet: uniform velocity of 1.14 m/s. Outlet: total pressure of 0 Pa. Symmetry plane along center line.
Wall roughness	0.001 m.
Multiphase settings	Multiphase model: Discrete phase model/Particle transport solid. Fluid pair model: One-way coupled. Sediment mass flow rate: 1000 kg/s. Sediment particle diameter: $D_{particle} \sim$ N (0.75 mm, 0.25 mm)
Solver controls	Advection scheme: High Resolution. Transient scheme: Second-Order Backward Euler.
Turbulence model	SAS–SST.
Convergence control	Maximum residuals for pressure, mass-momentum and turbulent parameters < 10^{-4}. Coefficient loops: 2–3 iterations.

Multiphase flow was implemented by enabling the particle transport solid model in CFX, also known as the discrete phase model (DPM). DPM uses the Eulerian–Lagrangian multiphase model to track the paths of individual particles as they travel through the domain. It is well-suited for situations such as in the present work, where the volume fraction of the solid phase is low. The one-way coupled fluid pair model was chosen to solve the fluid–particle interactions. This model is computationally cheaper than the two-way coupled model. As the sediment phase's effect on the fluid phase is negligible in this case, the one-way coupled model was found to produce satisfactory results. In the transient multiphase simulations, sediments were injected with uniform distribution over the inlet during the first 100 s. The mass flow of sediments was set to 1000 kg/s, leading to a total mass of sediments injected into the sand trap of 10^5 kg. The sediments were tracked as they travelled through the model, and the sand trap efficiency was given by the time-integrated mass flow report at the outlet by the end of the simulation. The sediment diameters have a normal distribution with a mean of 0.75 mm and a standard deviation of 0.25 mm.

By also ensuring that the solution is mesh independent, the accuracy of the results are further improved. Mesh independence is achieved when a defining value of the simulation no longer changes significantly. The purpose of a mesh-independence study is to minimise the discretisation error resulted from approximating the geometry during the meshing stage [18]. The model with both rakes and ribs was used for the mesh-independence study. Three different mesh qualities were used. Following the procedure described by Celik I. B. et al. [19], an estimation of the discretisation error was obtained. In the calculations, N is the number of cells; h is the representative cell size; r is the refinement factor; ϕ is the pressure drop from inlet to outlet; p is the apparent order of the method; ϕ_{ext} are the extrapolated values of ϕ; e_a and e_{ext} are the approximate and extrapolated relative errors, respectively; and $\mathrm{GCI}_{\mathrm{fine}}$ is the fine-grid convergence index. The mesh discretisation error was found to be 1.4%. The results of the calculations are presented in Table 2. The fine mesh with 26.9 million cells is considered for further analysis and will be used to conduct the final numerical studies.

Table 2. Parameters of the mesh-independence study.

Parameter	Value
N_1, N_2, N_3	26.9×10^6, 9.7×10^6, 4.3×10^6
h_1, h_2, h_3	0.08, 0.11, 0.14
r_{21}	1.4
r_{32}	1.3
ϕ_1	1838
ϕ_2	1860
ϕ_3	1897
p	2.1
ϕ_{ext}^{21}	1.8×10^3
e_a^{21}	0.0068%
e_{ext}^{21}	0.0458%
GCI_{fine}^{21}	1.4%

The simulation results are verified by ensuring that residuals reach a satisfactory convergence criteria and that there is a stable mass flow through the domain. This signifies that the solution is computationally correct. The hydraulic representation of the numerical model will be validated by comparison with PIV measurements on a physical scale model of the sand trap and to ADCP measurements from the prototype sand trap [4,20]. As the flow state is highly stochastic, the velocity distributions will never be identical. However, it is useful to make sure that the jet in the diffuser observed in the PIV measurements also exists in the simulated flow. It is also important to ensure that the simulated velocities are of reasonable magnitudes.

3. Results and Discussions

The results will mainly focus on how the velocity, vorticity, turbulence, and settling patterns vary between the three distinct models, as these are the key factors that affect sand trap efficiency in this case.

3.1. Sand Trap Efficiency

The sand trap efficiencies of the different models were obtained by creating a time-integrated particle mass flow report. This measures the total sediment mass entering the domain through the inlet and exiting through the outlet. The total time of 1000 s was found to be sufficient for all suspended sediments to exit the domain while remaining sediments are travelling along the bed. In the models with ribs implemented, sediments travelling along the bed are observed to pour into the gaps between ribs. At the end of simulation, not all sediments travelling along the bed have reached the ribs. However, a precedent is set by the sediments that do reach the ribs. These are all seen to pour into the the ribs instead of passing over them, indicating that this will also be the case for the remaining sediments. Due to limited computational resources, running the simulations for longer was not feasible. Running the simulations until all sediments are either completely settled or out of the domain could affect the sand trap efficiencies.

Using the model without upgrades as the base line, the mass of sediments exiting through the outlet is reduced by 24.5% from 2.5×10^3 to 1.9×10^3 kg by including the ribs. This indicates that the ribs are more effective at capturing and trapping bed load sediments than only the weir. By also adding the v-shaped rakes, the amount of sediments escaping the sand trap is increased by 48.5% from 2.5×10^3 to 3.7×10^3 kg compared with the model without upgrades. The amount of larger sediments trapped can be assumed to be similar before and after including the rakes, as larger sediments cannot be seen to escape the sand trap in neither particle track plots. The lack of performance from the model with rakes included can therefore be attributed to the turbulent vortices preventing smaller sediments to settle. This reduces sand trap efficiency. The sand trap efficiency of the different models are listed in Table 3.

Table 3. Sand trap efficiencies.

Model	Sediments Injected	Sediments Exited	Sand Trap Efficiency
No upgrades	10^5 kg	2.5×10^3 kg	97.5%
Ribs	10^5 kg	1.9×10^3 kg	98.1%
V-shaped rakes and ribs	10^5 kg	3.7×10^3 kg	96.3%

In all simulations, the divide between suspended load and bed load appears to be around 1 mm in diameter. The majority of sediments that remain suspended until escaping the sand trap are smaller than 1 mm, while the larger sediments travel along the bed by sliding, saltating, or rolling. Models for simulating sediment resuspension were not included in the simulations. The bed load sediments are therefore not observed to be resuspended. It has previously been shown that for classically dimensioned sand traps, sediment resuspension mostly occurs for sediments with grain sizes smaller than 2×10^{-4} m [21]. This is below the range of grain sizes used in the present work. Further analyses could be done with the resuspension models included and with smaller grain sizes to investigate the rate of sediment resuspension from the bed load. To further improve the sand trap efficiency, a flow calmer in the shape of horizontal bars, as suggested by Richter, should be tested. Instead of acting as a bluff body and inducing turbulence, this flow calmer could break up turbulence structures and improve settling characteristics for smaller sediments. Smoothing the transition between inlet and diffuser by reducing the inclination of the slope was suggested as an option to further increase the settling of smaller sediments [5]. However, it was found that this solution does not significantly improve the jet flow behaviour in the diffuser, thus not improving the settling of small sediments.

Looking at particle track plots of the different models, it appears that particles that reach the tunnel bed before passing over the ribs will indeed fall between them. This confirms the discovery from experiments by Richter et al. [4,5]. Sediments that remain suspended when passing the ribs will generally escape the sand trap. The amount of suspended sediments vary depending on if rakes are included in the diffuser or not. In the results where the rakes are not included, the suspended sediments are gathered closer towards the bottom of the tunnel. When rakes are included, the suspended sediments are of greater numbers and are more dispersed over the tunnel cross-section. This is believed to be caused by the turbulence from the rakes.

3.2. Head Losses

The head loss, Δh_L, of the different models was calculated from the steady-state simulations using the pressure-drop-based Darcy–Weisbach equation in Equation (3). The pressure difference, Δp, is calculated between the inlet and outlet faces of the models. Using the head loss in the model with no upgrades as a base value, the increased head loss caused by the upgrades was calculated by finding the difference in head loss between each of the upgraded models and the base value.

As presented in Table 4, the head loss caused by including just the ribs is 0.003 m, equating to an increase of 1.8% for the whole sand trap. Combined with the better sand trap efficiency of this model, this speaks for the value of including ribs in the sand trap. The model with both ribs and rakes included sees an increase in head loss of 12.7% compared to the model with no upgrades. The large head loss and the relatively poor sand trap efficiency of this model make it possible to conclude that other types of improvements to the sand trap should be pursued instead.

Table 4. Head loss, Δh_L, is calculated using Equation (3). Increased head loss is found by comparison with the model with no upgrades.

Model	Δh_L	Increased Head Loss
No upgrades	0.166 m	-
Ribs	0.169 m	0.003 m (+1.8%)
V-shaped rakes and ribs	0.187 m	0.021 m (+12.7%)

3.3. No Upgrades

The model with no upgrades represents the sand trap as it stands today, with a diffuser near the inlet and a weir just upstream of the penstock. The simulation results on the model with no upgrades give a baseline with which results from the other models can be compared. In addition, the results on this model will be compared to PIV and ADCP measurements for validation [4,5]. The velocity contour plot in Figure 5 shows the separation occurring at the entrance of the diffuser and the jet forming above it. Large circulation zones develop both in the horizontal and vertical planes at the entrance of the diffuser. These phenomena were obtained in both PIV results and in other experimental results, thus validating the simulations in this work [13,20]. Field measurements by Almeland et al. showed that the main current follows the centre of the diffuser, which can also be seen in the present results [12].

The turbulence, which develops from the separation in the diffuser, is seen to propagate through the sand trap, see Figure 6. The turbulence appears to dissipate as the flow reaches the halfway point before increasing as it crosses the weir and enters the penstock. The slow dissipation of turbulence may be due to the relative smoothness of the tunnel walls. Increasing the wall roughness to closer resemble the rough unlined tunnel walls in the prototype would affect the simulation results. One possibility is that turbulence would dissipate faster because of the increased energy losses. This would lead to improved sediment settling characteristics in the downstream end of the sand trap. Another possibility is that the rough walls may introduce even higher turbulence, disturbing sediment settling.

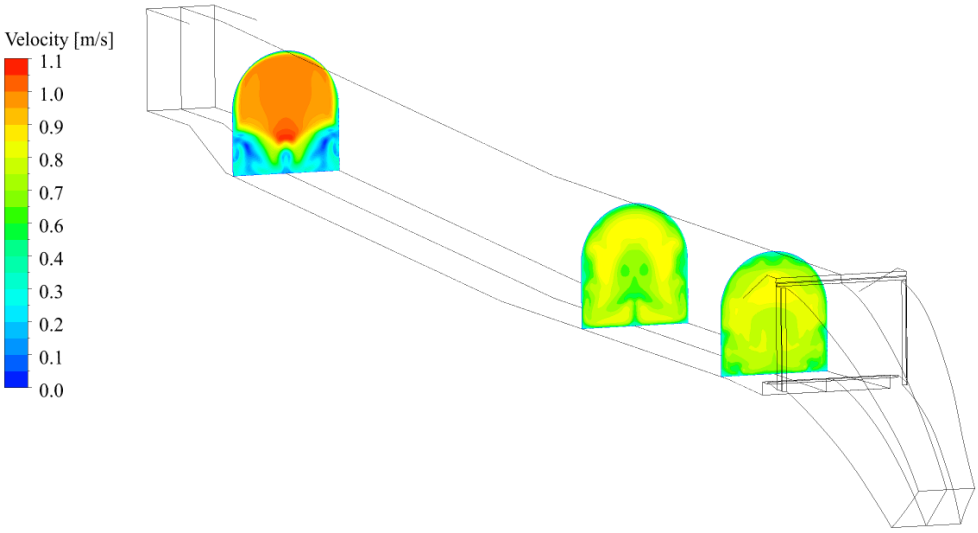

Figure 5. Velocity distributions in the sand trap with no upgrades included at t = 1000 s. A high-velocity jet above vortices caused by flow separation can be seen in the diffuser. Further downstream, the velocity is more evenly distributed.

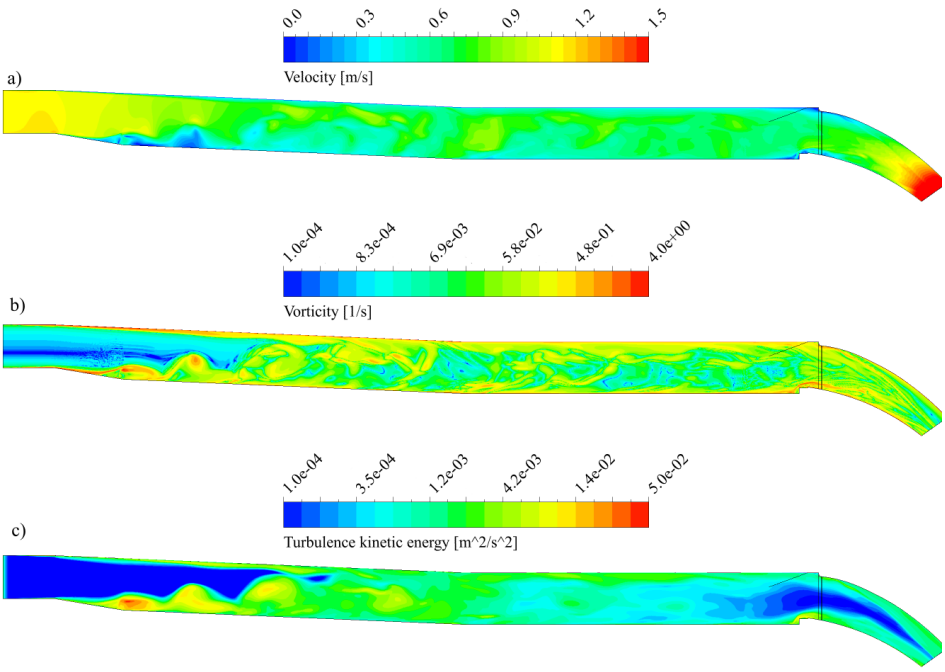

Figure 6. Sand trap without upgrades, symmetry plane at t = 1000 s. (**a**) Velocity contour. Flow separation occurs in the diffuser, which causes a higher flow velocity in the upper part of the diffuser. Separation is also seen to occur at the weir. (**b**) Vorticity contour. Flow separation in the diffuser and at the weir causes vortex generation. (**c**) Turbulence kinetic energy contour. Turbulence propagating from the diffuser starts to dissipate before reaching the penstock.

3.4. Sand Trap with Ribs

The flow behaviour upstream of the ribs remains identical to the model without upgrades. Large vortex structures propagate from the diffuser, where flow separation occurs. The separation of the flow field around the ribs is presented in Figure 7. This results in low velocities in the space below the ribs, which improves sediment settling. It can also be seen that inflow occurs at the last rib. This causes circulation in the downstream end of the space below the ribs. Sediments begin to settle in the upstream end, and will therefore be less affected by this circulation. However, this could change as the space fills up with

sediments. A turbulent boundary layer forms over the ribs from separation at the ramp. This will be beneficial for the settling of bed load sediments under the ribs, as these will slow down when entering the boundary layer. The chance of the sediments falling through the gaps is therefore increased. Flow into the penstock is more turbulent as a consequence of the turbulent boundary layer.

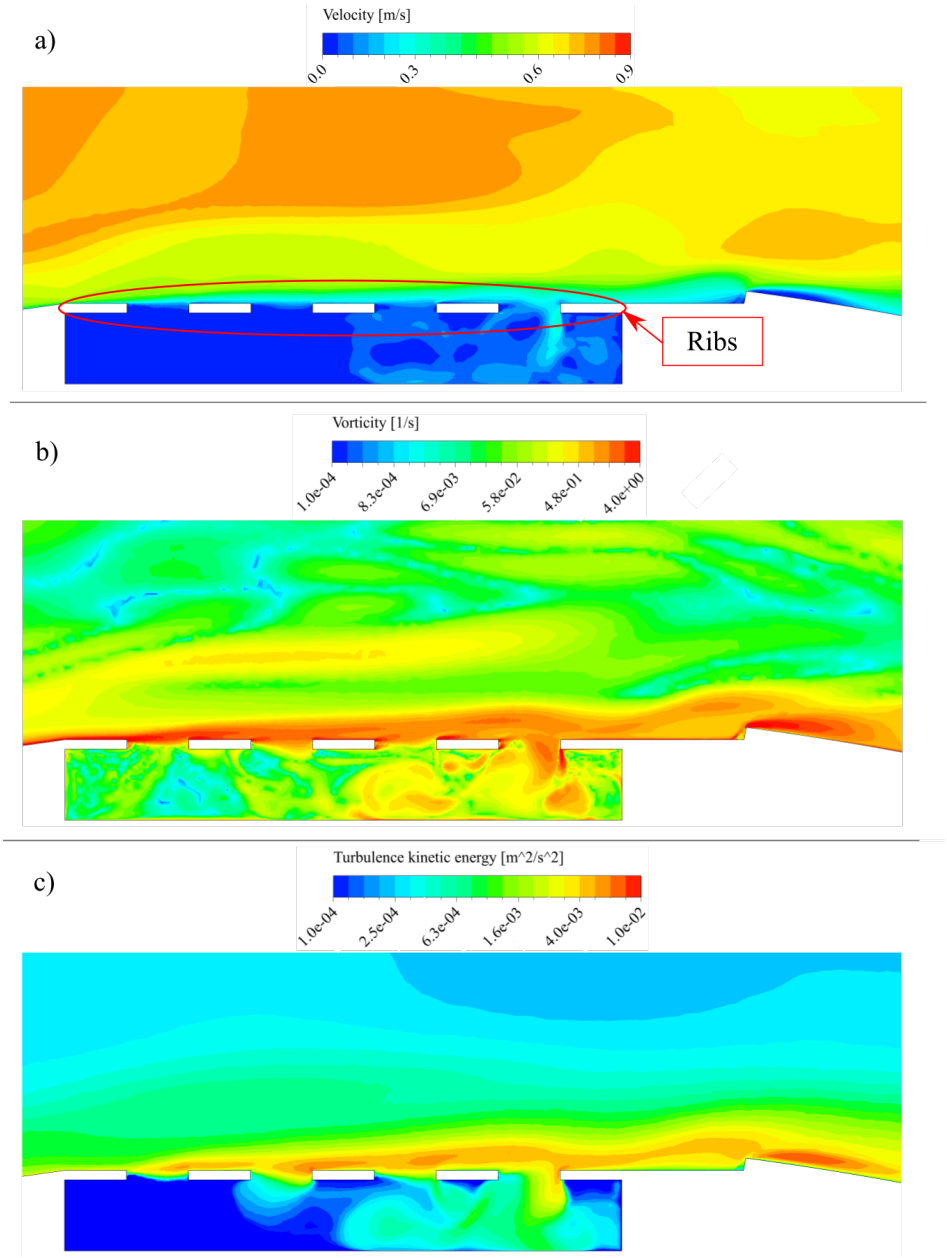

Figure 7. Extended view of ribs in the symmetry plane at t = 1000 s. (**a**) Velocity contour. Separation of the velocity field is visible. Low velocities below ribs increase the chances of sediment settling. Low-velocity inflow occurs between the last two ribs. This causes circulation in the downstream end below the ribs. Sediments will begin to settle in the upstream end, and will therefore be less affected by the circulation. However, this could change as the space fills up with sediments. (**b**) Vorticity contour. (**c**) Turbulence kinetic energy contour. A turbulent boundary layer forms over the ribs due to separation from the ramp. This will be beneficial for the settling of bed load sediments, as these will slow down when entering the boundary layer. Flow into the penstock is more turbulent as a consequence.

3.5. Sand Trap with Rakes and Ribs

It was hypothesised that the higher turbulence induced by the rakes would increase settling speed for larger sediment sizes. By studying the particle tracks in the simulation results, it can be seen from Figure 8 that sediments with a diameter larger than 1 mm tend to settle earlier in the sand trap compared with the geometries without the rakes in the diffuser. However, it can be observed that sediments smaller than 1 mm tend to remain suspended for longer when rakes are included. These smaller sediments have the potential to cause erosion damage on the turbine blades, and it is therefore desired to prevent these from escaping the sand trap.

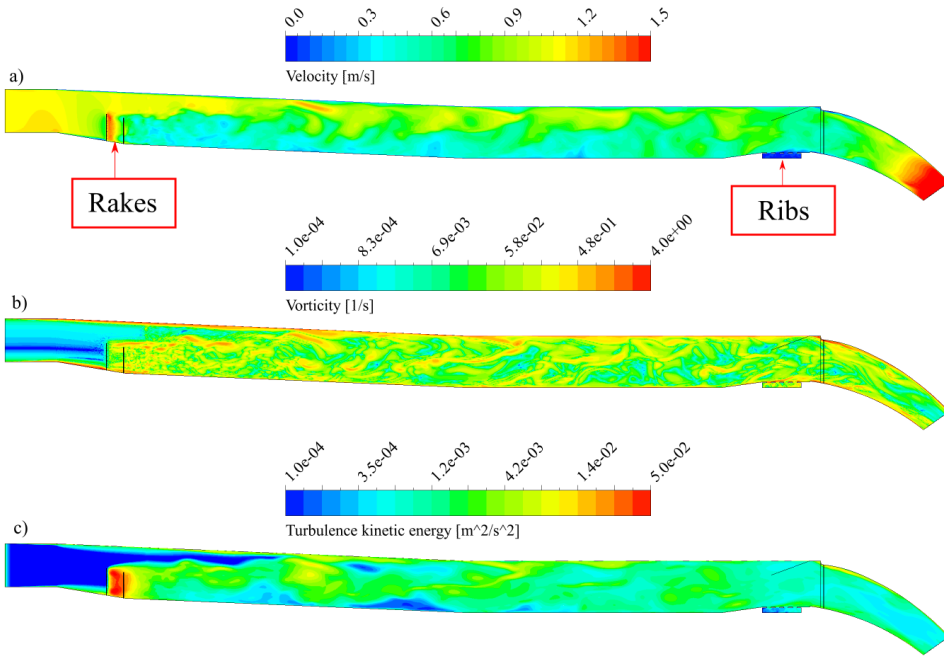

Figure 8. Sand trap with ribs and v-shaped rakes, symmetry plane at t = 1000 s. (**a**) Velocity contour. Flow over the rakes is accelerated, while flow going through the rakes slows down and becomes turbulent. (**b**) Vorticity contour. High vorticity appears immediately downstream of rakes and remains throughout the sand trap. (**c**) Turbulence kinetic energy contour. Rakes induce higher levels of turbulence than can be seen in models without rakes. Turbulence has not dissipated before the flow exits the sand trap

The large circulation zones, which also occur in the models without rakes, can be seen clearly in Figure 9. Sediments are seen to become trapped in these circulation zones in particle track plots. The flow is separated as it passes the rakes, where flow going over is accelerated, while flow going through decelerates and becomes turbulent. Vorticity and turbulence are induced by the vortex shedding at the rakes. The highest levels of turbulence are observed between the two rows of rakes. A large turbulent wake is established downstream of the rakes and remains until the outlet. In the present work, this has been shown to decrease sand trap efficiency. The flow downstream of the diffuser when rakes are included is seen to be more turbulent than when rakes are omitted. As the turbulence does not dissipate before exiting the sand trap, this causes more turbulent flow to enter the penstock.

If the height of the rakes was to be increased so that they reach the crown of the tunnel, it could affect the settling characteristics in multiple ways. One possibility is that increasing the height of the rakes would cause an earlier onset of turbulence and vorticity, which again carries small diameter sediments further. From the results in the present work, it is believed that this would lead to an increase in head loss and a decrease in sand trap efficiency. Another possibility is that the flow would no longer be divided into high- and

low-velocity zones downstream of the rakes. Instead, a general reduction in absolute flow velocity would occur. This could mean that the flow becomes more uniform, which might be beneficial for sand trap efficiency. In both cases, increasing the flow obstructing area is likely to increase head loss.

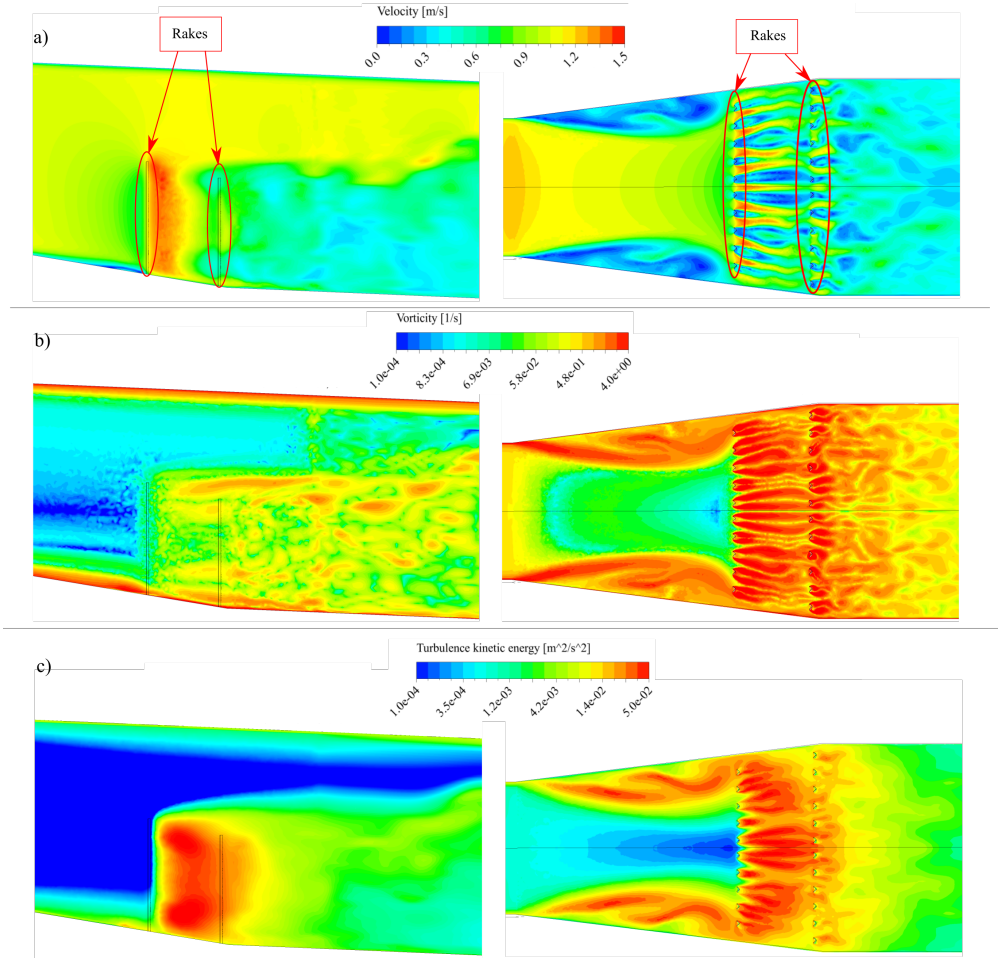

Figure 9. Extended view of v-shaped rakes in symmetry and horizontal planes at t = 1000 s. (**a**) Velocity contours. The large circulation zones, which can also be seen in the models without rakes, appear at the entrance of the diffuser. These zones are observed trapping sediments. Flow is separated going past the rakes. Flow going over is accelerated, while flow going through is decelerated. Velocity is highest between rakes. (**b**) Vorticity contours. Vorticity and turbulence is induced by the vortex shedding at the rakes. (**c**) Turbulence kinetic energy contours. The highest levels of turbulence are observed between the two rows of rakes. A large turbulent wake is established downstream of the rakes, which has been shown to decrease sand trap efficiency in the present work.

3.6. Consequences for Sand Trap Design

Based on the analysis results it is found that the tested rib design improves the trap efficiency and can be recommended for new sand traps and retrofitting of existing sand traps. The tested design was recently developed and presented in Richter et al. [5] and has not previously been installed in a hydropower plant. The tested v-shaped rakes were found to decrease the trap efficiency and, in addition, have a larger negative effect on the head loss. Such v-shaped rakes are installed in several existing hydropower plants, but this practice should be reconsidered. However, it is noted that only one design of the v-shaped rakes were tested and other designs may prove to have a positive effect on the trap efficiency.

4. Conclusions

It is necessary to minimise sediment erosion to increase the turbine's lifespan. Three-dimensional models based on the Tonstad power plant sand trap were created. Versions of the model include various upgrades to determine their effect on sediment settling. The numerical domain was discretised by a combination of hexahedral and tetrahedral mesh. Steady-state and transient multiphase simulations were performed on the models, using water and sand with a variable grain size. The objective was to investigate how installing rake- or rib-type structures affect particle sand trap efficiency and head loss.

By investigating the results, it was found that the sand trap with ribs at the outlet reduces the total weight of sediments exiting the sand trap by 24.5%, while increasing the head loss by around 1.8%. Installing rakes in the diffuser, although showing signs of increasing settling speed for larger sediments, was found to increase the total weight of sediments leaving the sand trap by 48.5%. This led to a reduced sand trap efficiency. In addition, the rakes caused an increased head loss of 12.7%. It is shown that in all models, sediments escaping the sand trap have a diameter smaller than one millimetre. These findings are supported by physical scale experiments on the sand trap [4,5,13]. The results show that installing ribs at the outlet of the sand trap will reduce sediment transport to the turbine and increase sand trap efficiency, thus prolonging turbine lifespan at the Tonstad power plant.

The main novelties from this work are the analysis results for the tested design of ribs and v-shaped rakes. The tested rib design has previously not been installed in a hydropower plant, and can be recommended based on the results in this work. The tested v-shaped rakes have been installed in existing hydropower plants previously, but this practice should be reconsidered.

For further work, running two-dimensional simulations along the centre line of the sand trap with the Large Eddy Simulation turbulence model could give a more accurate representation of the turbulence and sediment settling in the plane. Additional variants of the rakes should be tested to verify that they still have an adverse effect. The effects of extending the rakes to reach the crown of the tunnel so that the whole flow area is covered should also be investigated. Additionally, a model allowing for sediment resuspension should be explored to better represent sediments bouncing on or being resuspended from the bed. Further, experimental measurements of the inlet velocity profile are needed to create realistic and accurate inlet boundary conditions.

Author Contributions: Conceptualization, M.M.I., C.T. and K.V. methodology, M.M.I.; software, M.M.I.; formal analysis, M.M.I.; investigation, M.M.I.; resources, C.T.; data curation, M.M.I.; writing original draft preparation, M.M.I.; writing—review and editing, C.T. and K.V.; visualization, M.M.I.; supervision, C.T. and K.V.; project administration, C.T. All authors have read and agreed to the published version of the manuscript.

Funding: No funding is received for this work.

Institutional Review Board Statement: Not applicable.

Informed Consent Statement: Not applicable.

Conflicts of Interest: The authors declare no conflict interest.

1. References

1. Richter, W.; Vereide, K.; Zenz, G. Upgrading of a Norwegian pressurized sand trap combined with an open air surge tank. *Geomech. Tunn.* **2017**, *10*, 620–624. [CrossRef]
2. Truscott, G.F. A literature survey on abrasive wear in hydraulic machinery. *Wear* **1972**, *20*, 29–50. [CrossRef]
3. Thapa, B.S.; Thapa, B.; Dahlhaug, O.G. Current research in hydraulic turbines for handling sediments. *Energy* **2012**, *47*, 62–69. [CrossRef]
4. Vereide, K.; Richter, W.; Havrevoll, O.H.; Betete, K.; Shrestha, U.; Navaratnam, U.; Lia, L.; Mauko, G. *Flexible Sandtraps: Final Report (HydroCen Report)*; Technical Report; Norwegian Research Centre for Hydropower Technology: Trondheim, Norway, 2021; Volume 20.

5. Richter, W.; Mauko, G.; Zenz, G. *Hydraulic Investigation, Numerical and Physical Model Test, Flexible Sand Trap 2.0*; Technical Report; Graz University of Technology: Graz, Austria, 2020.
6. Maxey, M.R. The gravitational settling of aerosol particles in homogeneous turbulence and random flow fields. *J. Fluid Mech.* **1987**, *174*, 441–465. [CrossRef]
7. Wang, L.P.; Maxey, M.R. Settling velocity and concentration distribution of heavy particles in homogeneous isotropic turbulence. *J. Fluid Mech.* **1993**, *256*, 27–68. [CrossRef]
8. Aliseda, A.; Cartellier, A.; Hainaux, F.; Lasheras, J.C. Effect of preferential concentration on the settling velocity of heavy particles in homogeneous isotropic turbulence. *J. Fluid Mech.* **2002**, *468*, 77–105. [CrossRef]
9. Olsen, N.R.B.; Skoglund, M. Three-dimensional numerical modeling of water and sediment flow in a sand trap. *J. Hydraul. Res.* **1994**, *32*, 833–844. [CrossRef]
10. Olsen, N.R.B.; Kjellesvig, H.M. Three-dimensional numerical modelling of bed changes in a sand trap. *J. Hydraul. Res.* **1999**, *37*, 189–198. [CrossRef]
11. Bråtveit, K.; Olsen, N.R.B. Calibration of Horizontal Acoustic Doppler Current profilers by three dimensional CFD simulations. *Eng. Appl. Comput. Fluid Mech.* **2015**, *9*, 41–49. [CrossRef]
12. Almeland, S.K.; Olsen, N.R.B.; Bråveit, K.; Aryal, P.R. Multiple solutions of the Navier-Stokes equations computing water flow in sand traps. *Eng. Appl. Comput. Fluid Mech.* **2019**, *13*, 199–219. [CrossRef]
13. Havrevoll, O.H.; Vereide, K.; Rüther, N.; Lia, L. *PIV Experiments on Ribs in the Tonstad Rock Trap Model*; NTNU Reportno. B1-2021-2; Norwegian University of Science and Technology: Trondheim, Norway, 2021; p. 18.
14. Daxnerová, J. Hydraulic Scale Modelling of Flow Calming Structures for Hydropower Plants. Master's Thesis, NTNU, Trondheim, Norway, 2019.
15. Fergus, T.; Hoseth, K.A.; Sæterbø, E. *Vassdragshåndboka*, 1st ed.; Fagbokforlaget: Trondheim, Norway, 2010.
16. Menter, F.R.; Egorov, Y. The Scale-Adaptive Simulation Method for Unsteady Turbulent Flow Predictions. Part 1: Theory and Model Description. *Flow Turbul. Combust.* **2010**, *85*, 113–138. [CrossRef]
17. Davidson, L. The SAS Model: A Turbulence Model with Controlled Modelled dissipation. In Proceedings of the 20th Nordic Seminar on Computational Mechanics, Göteborg, Sweden, 20–23 November 2007.
18. Roache, P.J. Perspective: A Method for Uniform Reporting of Grid Refinement Studies. *J. Fluids Eng.* **1994**, *116*, 405–413. [CrossRef]
19. Celik, I.B.; Ghia, U.; Roache, P.; Freitas, C. Procedure for Estimation and Reporting of Uncertainty Due to Discretization in CFD Applications. *J. Fluids Eng.* **2008**, *130*. [CrossRef]
20. Brevik, O. *3D Numerisk Modellering av Deler av Vannvegen til Tonstad Kraftverk*; Institutt for vann-og miljøteknikk: Trondheim, Norway, 2013; Volume 139.
21. Ortmanns, C. Entsander von Wasserkraftanlagen. Ph.D. Thesis, ETH Zurich, Zurich, Switzerland, 2006.